HHS Public Access

Author manuscript

J Mech Behav Biomed Mater. Author manuscript; available in PMC 2019 December 01.

Published in final edited form as:

J Mech Behav Biomed Mater. 2018 December ; 88: 170–175. doi:10.1016/j.jmbbm.2018.08.023.

Load-Bearing Capacity of Lithium Disilicate and Ultra-Translucent Zirconias

Jing Yan, **Marina R. Kaizer**, and **Yu Zhang***

Department of Biomateirals & Biomimetics, New York University College of Dentistry, New York, New York 10010

Abstract

Objective: The aim of this study was to evaluate the load-bearing capacity of monolithic lithium disilicate (LiDi - IPS e.max CAD) and novel ultra-translucent zirconia restorative systems of various compositions: 5Y-PSZ (5 mol% yttria-partially-stabilized zirconia) and 4Y-PSZ (4 mol% yttria-partially-stabilized zirconia); relative to a 3Y-TZP (3 mol% yttria-stabilized zirconia) control.

Materials and methods: Experiments were carried out with 10 disc specimens (Ø12 × 1 mm) per ceramic material. The zirconia intaglio surface (as machined) was sandblasted (50 μm Al_2O_3 at 2 Bar), while LiDi was etched with 5% HF for 20 s. The ceramic discs were then adhesively bonded onto a dentin-like substrate (G10, a high-pressure fiberglass material) using Multilink Automix cement and Monobond Plus primer, producing a ceramic/cement/dentin-like substrate trilayer structure. The bonded specimens were stored in water for 3 days at 37°C prior to a Hertzian indentation flexural radial fracture test. The plate-on-foundation theory was used to validate the load-bearing capacity of the trilayer systems based on the flexural tensile stress at the ceramic intaglio (cementation) surface—a cause for bulk fracture of ceramic onlays.

Results: The experiment data showed that, when bonded to and supported by a dentin-like substrate, the load-bearing capacity of LiDi (872 N) is superior to the 5Y-PSZ (715 N) and can even reach that of 4Y-PSZ (864 N), while 3Y-TZP still holds the highest load-bearing capacity (1195 N). Theoretical analyses agree with experimental observations. The translucency of 5Y-PSZ approaches that of LiDi, which are superior to both 4Y-PSZ and 3Y-TZP.

Conclusions: When adhesively bonded to and supported by dentin, lithium disilicate exhibits similar load-bearing properties to 4Y-PSZ but much better than 5Y-PSZ.

Graphical Abstract

*Corresponding author: Yu Zhang, 433 First Avenue, Room 810, Department of Biomaterials and Biomimetics, New York University College of Dentistry, New York, NY 10010, Tel. +1 (212) 998-9637, yz21@nyu.edu.

Author Agreement/Declaration: All authors have seen and approved the final version of the manuscript being submitted. They warrant that the article is the authors' original work, hasn't received prior publication and isn't under consideration for publication elsewhere.

Conflict of Interest: All authors state that there is no financial/personal interest or belief that could affect our objectivity.

Declarations of interest: none

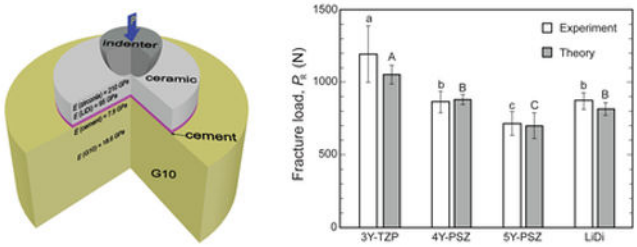

Keywords

Load-bearing capacity; Lithium disilicate; Ultra-translucent zirconia; Elastic modulus; Flexural strength; Layer thickness

1. Introduction

Monolithic dental restorations fabricated with CAD/CAM technology are gaining popularity among patients and practitioners due to their ease of fabrication and cost-effective characteristics (Li et al., 2014; Zhang and Kelly, 2017). The monolithic crowns in the posterior area of the mouth are mainly fabricated with two types of ceramics: lithia-based glass-ceramics or zirconia (yttria-stabilized polycrystals). Particular characteristics of these two classes of materials guide their clinical indications, as well as the clinicians preferences (Belli et al., 2017; Tong et al., 2016; Wendler et al., 2017; Zhang, 2014; Zhang and Lawn, 2018; Zhang et al., 2013a). The most widely used lithia-based glass-ceramic is lithium disilicate (LiDi), which is available in a variety of shades and opacities. Also, its glassy matrix allows for excellent bondability, using the traditional etch/silane technique. Nonetheless, these materials have only moderate strength (400 to 600 MPa) and toughness (2 to 2.5 $MPa.m^{1/2}$). On the other hand, traditional dental zirconia (3Y-TZP, 3 mol% yttria stabilized zirconia polycrystals) is the strongest (800 to 1200 MPa) and toughest (3.5 to 4.5 $MPa.m^{1/2}$) dental ceramic, but it is fairly opaque. The translucency of dental zirconia has been improved by increasing the yttria content. The novel ultra-translucent zirconias (4Y-PSZ and 5Y-PSZ, respectively, 4 mol% and 5 mol% yttria partially stabilized zirconia) have increased volume fractions of the optically isotropic cubic-phase (>50%), which have effectively increased the materials' translucency. However, the increase in cubic-content also results in reduced strength and toughness (Mao et al., 2018; Zhang et al., 2016a; Zhang and Lawn, 2018), likely to a level similar to that of LiDi.

Although the fracture resistance of ultra-translucent zirconia is significantly lower than that of traditional dental zirconia, their elastic modulus is the same (200 to 210 GPa), which is significantly higher than that of LiDi (95 to 105 GPa); both being stiffer than dental hard tissues (enamel ~70 GPa and dentin ~18 GPa) (Kinney et al., 2003; Poolthong et al., 1998; Zhang and Lawn, 2018). It's well known that the elastic modulus mismatch between ceramic and supporting structure influences the load-bearing capacity of the ceramic (Timoshenko and Woinowsky-Krieger, 1959). The same is valid for dental ceramic restorations when supported by dental structures (Zhang et al., 2009). A previous finite element analysis (Ma et al., 2013) showed that although the flexural strength of zirconia

(3Y-TZP) is 2.5 times higher than that of the LiDi glass-ceramic, the difference in load-bearing property is significantly reduced when these materials are bonded to enamel supported by dentin. Therefore, we hypothesize that LiDi should have similar or even superior load-bearing capacity to that of novel ultra-translucent zirconias, owing to their similar flexural strength but smaller elastic mismatch between LiDi and dental hard tissues relative to zirconias. This study experimentally evaluated the load-bearing capacity of LiDi and zirconia bonded onto a dentin-like substrate, which was validated by the plate-on-foundation theory.

2. Materials and methods

2.1 Materials and sample preparation

Disc-shaped specimens (Ø12 mm × 1 mm thickness, final dimensions) were prepared from three dental zirconias (the Luxisse series; Heany Industries, USA) and lithium disilicate (IPS e.max CAD; Ivoclar Vivadent, Lichtenstein). The surface of each disc was grinded dry after cutting, using a 320-grit (~35 μm) silicon carbide paper, to simulate the surface produced by CAD/CAM milling. Descriptions of the materials and sintering temperatures are given in Table I. The microstructure of these materials was observed on highly polished (0.5 μm) and thermally etched (zirconia) or acid etched (LiDi) samples by field emission scanning electron microscopy (Zeiss Merlin FE-SEM). To prevent grain growth, thermal etching was carried out at a relatively low temperature (1250°C for 20 min) and fast heating rate (20°C/min). For grain size analysis, at least 300 grains were measured using the linear intercept method (ASTM Standard E112, 2013). A correction factor of 1.56 for tetrakaidecahedral grains was used (Wurst and Nelson, 1972).

2.2 Fracture resistance experiments

The free-standing biaxial strength of each material ($n = 10$) was determined by the piston-on-three-balls test, using a loading rate of 1 mm/min, following the ISO 6872 (ISO/FDIS 6872, 2015).

To simulate the fracture resistance of ceramic prostheses supported by tooth dentin, ceramic specimens of each material ($n = 10$) were bonded to a dentin-like substrate (G10, Acculam, USA). G10 is a glass fiber reinforced epoxy resin, with elastic modulus $E = 18.6$ GPa similar to human dentin (Kinney et al., 2003). G10 rods were flattened and finished with 45 μm diamond grinding, then soaked in water for 21 days for complete hydration.

For adhesive bonding, the G10 surface was acid etched (5% HF for 2 min), while the zirconia intaglio surface was sandblasted (50 μm Al_2O_3 at 2 Bar), and LiDi was acid etched (5% HF for 20 s), following recommended protocols for their clinical use. After that, all samples were cleaned in an ultrasonic water bath for 2 min and dried. Adhesive bonding was carried out using Multilink Automix cement and Monobond Plus primer (Ivoclar Vivadent, Amherst, NY). A static load of 1 kg was used for 120 s to standardize cement thickness. The samples were then light cured for 4 intervals of 30 s at directions 90° apart. The ceramic/cement/G10 trilayer specimens were stored in water for 3 days at 37°C to allow the continuous polymerization and complete hydration of the cement layer prior to the Hertzian

load-to-fracture test. The fracture resistance test was performed by loading the ceramic/cement/G10 trilayer specimens at the top ceramic surface with a rigid tungsten carbide (WC) indenter (r = 3.18 mm) under the loading rate of 1 mm/min. It is true that the elastic modulus of WC is 3 times that of the stiffest opposing ceramic prostheses. The theory of contact mechanics and our previous study (Ma et al., 2013) have shown that although the elastic modulus of the indenter has profound influence on the initiation of the near-contact cone cracks, it has little effect on the onset of the far-field flexural radial cracks. To suppress the formation of cone cracks and to achieve a uniform force distribution, a thin piece of nitrile foil was placed between the ceramic surface and the loading ball. The schematic of the test configuration along with the specimen geometric parameters is shown in Fig. 1. Critical load for the onset of radial fracture was registered. All ceramic discs were then carefully peeled off of their G10 substrate for optical microscopy examination. By using a combination of reflected and transmitted light illumination, it was possible to confirm that the fracture does indeed originate from the cementation radial cracks and not from the near-contact cone cracks.

2.3 Plate-on-foundation theory

The plate-on-foundation theory was used to predict the theoretical load-bearing capacity of the trilayer systems (ceramic/cement/dentin-like substrate) according to their elastic gradients (Fig. 1).

Critical load (P_R) for the onset of radial fracture from the ceramic intaglio surface was calculated by the plate (ceramic restoration) on foundation (cement/dentin assembly) theory. The mathematical model is composed of three equations (Kim et al., 2003; Timoshenko and Woinowsky-Krieger, 1959):

$$P_R = \frac{B\sigma d^2}{\log\left(\frac{CE}{E^*}\right)} \quad (1)$$

where E is the flexural modulus of the ceramic, zirconia (= 210 GPa) and lithium disilicate (= 95 GPa) (Ma et al., 2013); σ is the flexural strength of the ceramic, which was investigated in this study (Table I); d is the thickness of the ceramic. C (≈ 1) and B (= 1.35) are the dimensionless constants (Miranda et al., 2003); E* is the effective modulus of the cement/dentin (G10) layer which is based on contact mechanics (Gao et al., 1992; Hu and Lawn, 1998; Kim et al., 2003):

$$E^* = E_c\left(\frac{E_s}{E_c}\right)^L \quad (2)$$

where E_s and E_c are the modulus of cement (7.9 GPa scientific document from Ivoclar) and dentin-like substrate (18.6 GPa), and L is an experimentally determined dimensionless function which is described by equation (3) (Kim et al., 2003):

$$L = \exp\left\{-\left[\alpha + \beta\, log\left(\frac{h}{d}\right)\right]^{\gamma}\right\} \quad (3)$$

where $\alpha = 1.18$, $\beta = 0.33$, $\gamma = 3.13$ (Kim et al., 2003); and h is the thickness of cement measured in cross-sectioned specimens (~ 40 μm).

2.4 Translucency parameter and contrast ratio

Highly polished (0.5 μm diamond grits) disc specimens ($n = 3$) were measured by a calibrated dental colorimeter (SpectroShade Micro; MHT). Color coordinates CIE$L^*a^*b^*$ were measured over standard backgrounds (black $L^* = 1.8$, $a^* = 1.3$, $b^* = -1.5$ and white $L^* = 95.7$, $a^* = -1.3$, $b^* = 2.6$). To ensure optical continuity, a drop of glycerol ($n = 1.472$) was placed between the specimen and background (Nogueira and Della Bona, 2013).

The translucency parameter (TP) of the material can be determined by the color difference between the specimen on black (B) and white (W) backgrounds (Kaizer et al., 2017):

$$TP = \sqrt{\left(L_B^* - L_W^*\right)^2 + \left(a_B^* - a_W^*\right)^2 + \left(b_B^* - b_W^*\right)^2} \quad (4)$$

where L^*, a^*, and b^* refer respectively to the lightness, redness to greenness, and yellowness to blueness coordinates in the CIE color space (CIE, 2004).

CR is the ratio of spectral reflectance of the light (Y) of the specimen on black (Y_B) and white (Y_W) backgrounds (Nogueira and Della Bona, 2013):

$$CR = \frac{Y_B}{Y_W} \quad (5)$$

$$Y = \left(\frac{L^* + 16}{116}\right)^3 Y_n \quad (6)$$

The specified white stimulus (Y_n) is normally chosen since it is a perfect reflecting diffuser, that is, $Y_n = 100$. CR values range from 0 (for a transparent material) to 1 (for a totally opaque material).

2.5 Statistical analyses

Four outcomes were investigated in this study: Flexural strength, Load-bearing capacity, translucency parameter, and contrast ratio. Data for each outcome was separately analyzed for normality and equality of variances, and then subjected to 1-way analysis of variance (ANOVA). Multiple comparisons were performed using the Tukey test. The significance level was set at 5%.

3. Results

The SEM images of thermally etched zirconias and acid etched LiDi are shown in Figure 2. The zirconia average grain size was 1.33 ± 0.06 μm for 5Y-PSZ, 0.95 ± 0.03 μm for 4Y-PSZ, and 0.54 ± 0.04 μm for 3Y-TZP. The glass-ceramic consisted of ~70 vol% elongated LiDi crystals. The average grain size of LiDi crystals was 1 to 3 μm in length and 0.1 to 0.4 μm in width.

Table 1 also summarizes the composition, mechanical properties and layer thicknesses of various ceramic materials, luting cement, and a dentin analogue material used in the present study. The piston-on-3-ball biaxial flexural strength of the ceramic prosthetic materials, and the elastic modulus and thickness of material of each layer (Fig. 1) were used to predict the critical fracture load of the ceramic/cement/G10 trilayer systems by the plate-on-foundation theory (Eqs. 1 – 3). It is important to note that the biaxial strength of LiDi was similar to that of 5Y-PSZ but lower than 4Y-PSZ, while 3Y-TZP remained the strongest among all materials. In addition, the elastic modulus of LiDi (95 GPa) was only half of that of the zirconias (210 GPa), making it much more compatible with the dentin-like substrate (18.6 GPa).

Rietveld refinement on XRD spectra using MAUD revealed that 5Y-PSZ is comprised of approximately 69% *c*-ZrO_2 and 31% *t*-ZrO_2, whereas 4Y-PSZ and 3Y-TZP consist of 57% *c*-ZrO_2 and 43% *t*-ZrO_2 and 29% *c*-ZrO_2 and 71% *t*-ZrO_2, respectively. On the other hand, LiDi consists of a dominant lithium disilicate phase ($Li_2Si_2PO_5$) couple with a subordinate lithium phosphate phase (Li_3PO_4) embedded in a glass matrix.

Fracture modes in ceramic layers subjected to the Hertzian load-to-fracture test are shown in Fig. 3. Stereo optical microscopy examination of the specimen surface using reflected light illumination revealed an absence of the formation of near-contact induced cone cracks in all cases [Figs. 3(a) and (c)]. Note: arrows in (a) and (c) indicate the contact area. However, stereo optical microscopy examination of the same specimens using transmitted light illumination revealed the far-field flexural induced radial cracks [Figs. 3(b) and (d)], suggesting that fracture is indeed initiated from the cementation surface of the ceramic discs.

Fig. 4 shows that, when bonded to and supported by dentin, the load-bearing capacity of LiDi can reach that of its 4Y-PSZ counterpart, and is much higher than 5Y-PSZ. Nonetheless, 3Y-TZP holds the highest load-bearing capacity (1195 ± 195 N) among the materials tested. Theoretical predictions for critical fracture load were found to agree very well with experimental results.

Fig. 5 depicts the *TP* and *CR* results for the materials tested of a common thickness 1 mm. 5Y-PSZ has the highest translucency among the zirconias, and approaches that of LiDi. These findings are further supported by a comparative digital photography.

4. Discussion

Due to the superior mechanical properties and ease of fabrication in CAD/CAM systems, zirconia and lithium disilicate have already become the materials of choice for posterior all

ceramic restorations (Rekow et al., 2011; Zhang, 2012). From the biaxial flexural test, we found that lithium disilicate has similar flexural strength (488 MPa) to 5Y-PSZ (593 MPa), whereas 4Y-PSZ and 3Y-TZP are around 1.5 and 2 times, respectively, stronger than lithium disilicate. Our findings suggest that zirconias, particularly 3Y-TZP and 4Y-PSZ, are much more suitable for freestanding stress-bearing applications, such as a multi-unit or long span fixed partial prosthesis (Pjetursson et al., 2015; Zhang and Ma, 2009).

When these ceramic restorative materials are bonded to and supported by dentin, the rank of load-bearing capacity can change, due primarily to the difference in key mechanical property E in conjunction with layer thicknesses d (ceramic restoration) and h (luting cement). From the perspective of ceramic restorative materials, a high elastic modulus ceramic plate provides protection for the underline tooth structure by bearing the (occlusal) contact stress (stress shielding) (Dejak et al., 2012; Zhang et al., 2016b). This, however, makes the ceramic restoration more prone to flexural damage, especially for low strength materials with small thicknesses. For this reason, high modulus and low strength ceramics, such as alumina (which has a modulus twice as high as zirconia but a strength only half of that of zirconia), are much more prone to flexural fracture relative to zirconia (Christensen and Ploeger, 2010; Selz et al., 2014).

From the perspective of the cement/dentin foundation, a higher elastic modulus foundation offers better support for the ceramic plate by preventing ceramic flexure upon (occlusal) contact loading (Ma et al., 2013; Rojpaibool and Leevailoj, 2017). It is important to note that the elastic modulus of the foundation is an effective (or combined) modulus of the cement layer and dentin analogue substrate. Since the modulus of most commercial luting cements ($E_c \sim 2 – 10$ GPa) is much lower than the modulus of dentin and enamel, it is essential to keep the thickness of the cement layer small in order to achieve a high foundation modulus. A thin cement layer is beneficial not only to improve the load-bearing capacity, but also to ensure an adequately fitted restoration.

Now consider a ceramic/cement/dentin trilayer system, the load-bearing property of the ceramic restoration is governed not only by its strength and thickness but also the elastic modulus mismatch between the ceramic plate and cement/dentin foundation. Although the dependence of the fracture load on the modulus mismatch is the logarithm to base 10 of the plate to foundation modulus ratio, in the case of ceramic modulus approaches to that of the tooth support, the effect of modulus mismatch on the load-bearing property can be significant (Eq. 1). Therefore, the key for achieving long-term stability of ceramic restorations supported by tooth structures is to select a high strength and low modulus ceramic material, minimize the luting cement thickness, and wherever it is possible, preserve the enamel structure. The higher elastic modulus of enamel coupled with its better resin bonding ability relative to dentin can further increase the load-bearing property and longevity of ceramics (Layton and Clarke, 2013; Layton et al., 2012; Rojpaibool and Leevailoj, 2017).

We acknowledge that this study has several limitations. All ceramic restorations are susceptible to premature fracture under cyclic fatigue loading (Wendler et al., 2018; Zhang et al., 2013b). In the case of radial fracture due to flexural stresses at the ceramic intaglio

surface, loss of load-bearing capacity is predominantly due to moisture assisted slow crack growth (SCG) (Bhowmick et al., 2005; Ramos Nde et al., 2016). Although all oxide ceramics are susceptible to SCG, the crack velocity exponent for LiDi (20 ± 3) is smaller than that of zirconia (25 ± 2), indicating that LiDi would exhibit faster degradation of load-bearing property relative to zirconia (Zhang and Lawn, 2004). It is important to note that the velocity exponent values cited here was determined from ceramic plates on compliant substrates, which had already considered foundation (cement/dentin-like substrate) creep induced loading rate effects on the onset of radial cracks (Huang et al., 2007).

Dental restorations often have significant curvatures at the cementation intaglio surface (Rekow et al., 2009). Studies from our labs (Kim et al., 2009) and elsewhere (Qasim et al., 2005; Rudas et al., 2005) have shown that flexural radial cracks require a higher load to initiate in the curved structures relative to their flat counterparts. However, these radial cracks can propagate rapidly to the margins of the curved specimens. In addition, curved structures are also more prone to contact induced cone cracks, which can potentially result in restoration chipping (Kim et al., 2009).

5. Conclusions

When adhesively bonded to a dentin-like support, lithium disilicate restorations exhibit similar load-bearing properties to that of new ultra-translucent zirconias (i.e. 4Y- and 5Y-PSZ), suggesting that lithium disilicate glass-ceramics have great potential for durable and esthetic minimally invasive restorations. In the case of the 3 zirconia materials, there exists a tradeoff between the load bearing property and translucency. 5Y-PSZ is most translucent (being only slightly below that of lithium disilicate), whereas 3Y-TZP possesses the best load-bearing capacity. 4Y-PSZ occupies the middle ground.

Acknowledgements

The authors would like to thank Prof. Do Kyung Kim and Dr. Minglei Zhao for XRD analyses, and Dr. Jingxiang Yang for SEM characterizations (Figs. 2a and c). This work was supported by National Institutes of Health (grant number. R01DE026772 and R01DE026279).

References:

ASTM Standard E112, 2013 Standard Test Methods for Determining Average Grain Size ASTM International, West Conshohocken, PA, 2013, DOI: 10.1520/E0112.

Belli R, Wendler M, de Ligny D, Cicconi MR, Petschelt A, Peterlik H, Lohbauer U, 2017 Chairside CAD/CAM materials. Part 1: Measurement of elastic constants and microstructural characterization. Dent Mater 33, 84–98. [PubMed: 27890354]

Bhowmick S, Zhang Y, Lawn BR, 2005 Competing fracture modes in brittle materials subject to concentrated cyclic loading in liquid environments: Bilayer structures. J Mater Res 20, 2792–2800.

Christensen RP, Ploeger BJ, 2010 A clinical comparison of zirconia, metal and alumina fixed-prosthesis frameworks veneered with layered or pressed ceramic: a three-year report. J Am Dent Assoc 141, 1317–1329. [PubMed: 21037189]

CIE, 2004 Technical Committee: Colorimetry. CIE pub no 15.3. Vienna, Austria: CIE Central Bureau.

Dejak B, Mlotkowski A, Langot C, 2012 Three-dimensional finite element analysis of molars with thin-walled prosthetic crowns made of various materials. Dent Mater 28, 433–441. [PubMed: 22209573]

Gao HJ, Chiu CH, Lee J, 1992 Elastic Contact Versus Indentation Modeling of Multilayered Materials. Int J Solids Struct 29, 2471–2492.

Hu XZ, Lawn BR, 1998 A simple indentation stress-strain relation for contacts with spheres on bilayer structures. Thin Solid Films 322, 225–232.

Huang M, Niu X, Soboyejo WO, 2007 Creep induced rate effects on radial cracks in multilayered structures. J Mater Sci Mater Med 18, 65–69. [PubMed: 17200815]

ISO/FDIS 6872, 2015 Dentistry - Ceramic materials Interanational Standard Organization, PO Box 56 • CH-1211 Geneva 20, Switzerland.

Kaizer MR, Gierthmuehlen PC, Dos Santos MB, Cava SS, Zhang Y, 2017 Speed sintering translucent zirconia for chairside one-visit dental restorations: Optical, mechanical, and wear characteristics. Ceram Int 43, 10999–11005. [PubMed: 29097830]

Kim JH, Miranda P, Kim DK, Lawn BR, 2003 Effect of an adhesive interlayer on the fracture of a brittle coating on a supporting substrate. J Mater Res 18, 222–227.

Kim JW, Thompson VP, Rekow ED, Jung YG, Zhang Y, 2009 Fracture Modes in Curved Brittle Layers Subject to Concentrated Cyclic Loading in Liquid Environments. J Mater Res 24, 1075–1081. [PubMed: 26028811]

Kinney JH, Marshall SJ, Marshall GW, 2003 The mechanical properties of human dentin: a critical review and re-evaluation of the dental literature. Crit Rev Oral Biol Med 14, 13–29. [PubMed: 12764017]

Layton DM, Clarke M, 2013 A systematic review and meta-analysis of the survival of non-feldspathic porcelain veneers over 5 and 10 years. Int J Prosthodont 26, 111–124. [PubMed: 23476903]

Layton DM, Clarke M, Walton TR, 2012 A systematic review and meta-analysis of the survival of feldspathic porcelain veneers over 5 and 10 years. Int J Prosthodont 25, 590–603. [PubMed: 23101039]

Li RW, Chow TW, Matinlinna JP, 2014 Ceramic dental biomaterials and CAD/CAM technology: state of the art. J Prosthodont Res 58, 208–216. [PubMed: 25172234]

Ma L, Guess PC, Zhang Y, 2013 Load-bearing properties of minimal-invasive monolithic lithium disilicate and zirconia occlusal onlays: finite element and theoretical analyses. Dent Mater 29, 742–751. [PubMed: 23683531]

Mao L, Kaizer MR, Zhao M, Guo B, Song YF, Zhang Y, 2018 Graded Ultra-Translucent Zirconia (5Y-PSZ) for Strength and Functionalities. J Dent Res e-print, 1–7.

Miranda P, Pajares A, Guiberteau F, Deng Y, Lawn BR, 2003 Designing damage-resistant brittle-coating structures: I. Bilayers. Acta Mater 51, 4347–4356.

Nogueira AD, Della Bona A, 2013 The effect of a coupling medium on color and translucency of CAD-CAM ceramics. J Dent 41 Suppl 3, e18–23. [PubMed: 23438417]

Pjetursson BE, Sailer I, Makarov NA, Zwahlen M, Thoma DS, 2015 All-ceramic or metal-ceramic tooth-supported fixed dental prostheses (FDPs)? A systematic review of the survival and complication rates. Part II: Multiple-unit FDPs. Dent Mater 31, 624–639. [PubMed: 25935732]

Poolthong S, Swain MV, Mori T, 1998 Ultra micro-indentation of tooth using spherical and triangular indenters. J Dent Res 77, 1129–1129.

Qasim T, Bush MB, Hu X, Lawn BR, 2005 Contact damage in brittle coating layers: influence of surface curvature. J Biomed Mater Res B Appl Biomater 73, 179–185. [PubMed: 15625677]

Ramos Nde C, Campos TM, Paz IS, Machado JP, Bottino MA, Cesar PF, Melo RM, 2016 Microstructure characterization and SCG of newly engineered dental ceramics. Dent Mater 32, 870–878. [PubMed: 27094589]

Rekow ED, Silva NR, Coelho PG, Zhang Y, Guess P, Thompson VP, 2011 Performance of dental ceramics: challenges for improvements. J Dent Res 90, 937–952. [PubMed: 21224408]

Rekow ED, Zhang G, Thompson V, Kim JW, Coehlo P, Zhang Y, 2009 Effects of geometry on fracture initiation and propagation in all-ceramic crowns. J Biomed Mater Res B Appl Biomater 88, 436–446. [PubMed: 18506827]

Rojpaibool T, Leevailoj C, 2017 Fracture Resistance of Lithium Disilicate Ceramics Bonded to Enamel or Dentin Using Different Resin Cement Types and Film Thicknesses. J Prosthodont 26, 141–149. [PubMed: 26505488]

Rudas M, Qasim T, Bush MB, Lawn BR, 2005 Failure of curved brittle layer systems from radial cracking in concentrated surface loading. J Mater Res 20, 2812–2819.

Selz CF, Strub JR, Vach K, Guess PC, 2014 Long-term performance of posterior InCeram Alumina crowns cemented with different luting agents: a prospective, randomized clinical split-mouth study over 5 years. Clin Oral Investig 18, 1695–1703.

Timoshenko S, Woinowsky-Krieger S, 1959 Theory of plates and shells. New York: McGraw-Hill 2nd ed.

Tong H, Tanaka CB, Kaizer MR, Zhang Y, 2016 Characterization of three commercial Y-TZP ceramics produced for their High-Translucency, High-Strength and High-Surface Area. Ceram Int 42, 1077–1085. [PubMed: 26664123]

Wendler M, Belli R, Petschelt A, Mevec D, Harrer W, Lube T, Danzer R, Lohbauer U, 2017 Chairside CAD/CAM materials. Part 2: Flexural strength testing. Dent mater 33, 99–109. [PubMed: 27884403]

Wendler M, Belli R, Valladares D, Petschelt A, Lohbauer U, 2018 Chairside CAD/CAM materials. Part 3: Cyclic fatigue parameters and lifetime predictions. Dent Mater.

Wurst JC, Nelson JA, 1972 Lineal Intercept Technique for Measuring Grain Size in Two-Phase Polycrystalline Ceramics. J Am Ceram Soc 55, 109–109.

Zhang F, Inokoshi M, Batuk M, Hadermann J, Naert I, Van Meerbeek B, Vleugels J, 2016a Strength, toughness and aging stability of highly-translucent Y-TZP ceramics for dental restorations. Dent Mater 32, e327–e337. [PubMed: 27697332]

Zhang Y, 2012 Overview: Damage resistance of graded ceramic restorative materials. J Eur Ceram Soc 32, 2623–2632. [PubMed: 22778494]

Zhang Y, 2014 Making yttria-stabilized tetragonal zirconia translucent. Dent Mater 30, 1195–1203. [PubMed: 25193781]

Zhang Y, Kelly JR, 2017 Dental Ceramics for Restoration and Metal Veneering. Dent Clin North Am 61, 797–819. [PubMed: 28886769]

Zhang Y, Kim JW, Bhowmick S, Thompson VP, Rekow ED, 2009 Competition of fracture mechanisms in monolithic dental ceramics: flat model systems. J Biomed Mater Res B Appl Biomater 88, 402–411. [PubMed: 18478533]

Zhang Y, Lawn B, 2004 Long-term strength of ceramics for biomedical applications. J Biomed Mater Res B Appl Biomater 69, 166–172. [PubMed: 15116406]

Zhang Y, Lawn BR, 2018 Novel Zirconia Materials in Dentistry. J Dent Res 97, 140–147. [PubMed: 29035694]

Zhang Y, Lee JJ, Srikanth R, Lawn BR, 2013a Edge chipping and flexural resistance of monolithic ceramics. Dent Mater 29, 1201–1208. [PubMed: 24139756]

Zhang Y, Ma L, 2009 Optimization of ceramic strength using elastic gradients. Acta Mater 57, 2721–2729. [PubMed: 20161019]

Zhang Y, Mai Z, Barani A, Bush M, Lawn B, 2016b Fracture-resistant monolithic dental crowns. Dent Mater 32, 442–449. [PubMed: 26792623]

Zhang Y, Sailer I, Lawn BR, 2013b Fatigue of dental ceramics. J Dent 41, 1135–1147. [PubMed: 24135295]

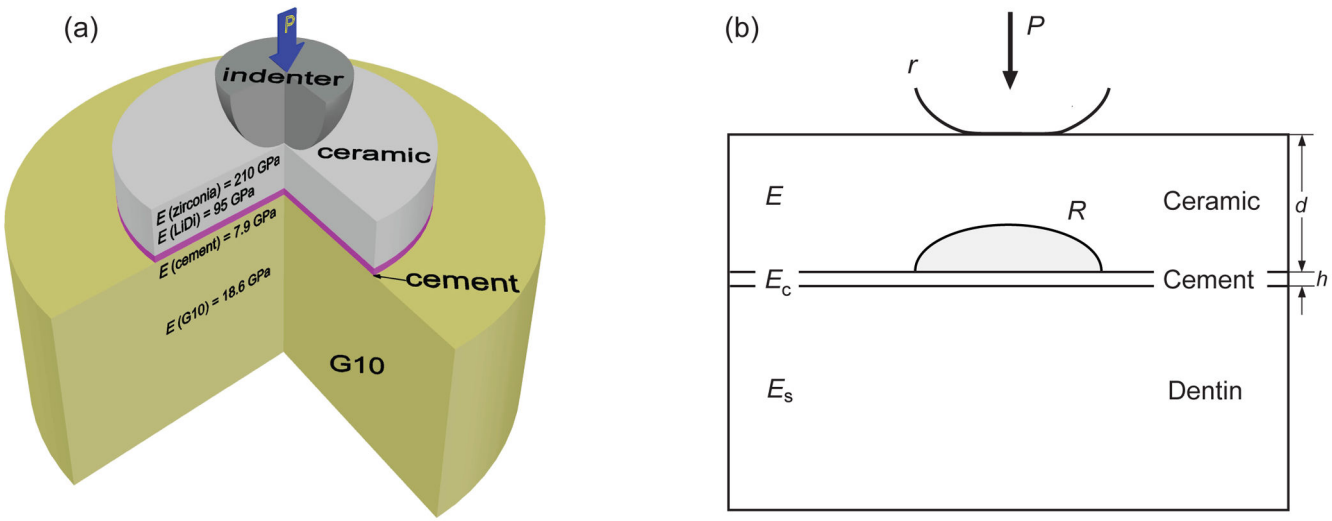

Figure 1.

Schematic of the Hertzian load-to-fracture test configuration used to determine the critical load of radial crack.

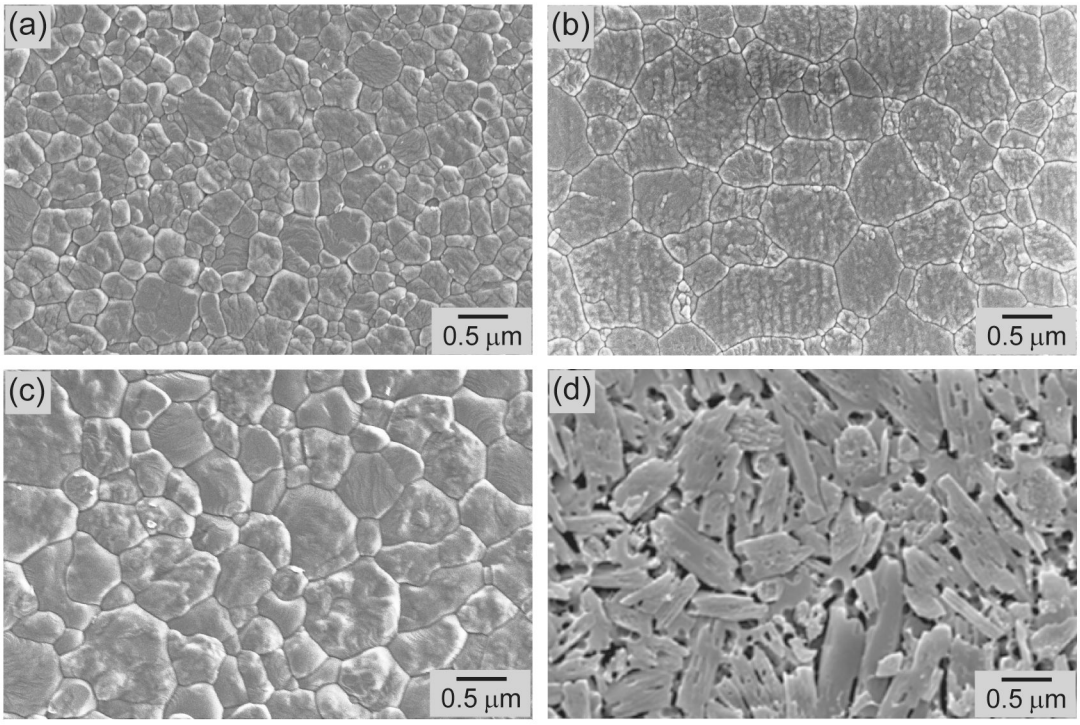

Figure 2.

The zirconias are polycrystalline ceramics, with (a) 3Y-TZP having average crystal size of 0.54 ± 0.04 μm, (b) 4Y-PSZ 0.95 ±0.03 μm, and (c) 5Y-PSZ 1.33 ± 0.06 μm. (d) IPS e.max CAD is a glass ceramic composed of ~70% lithium disilicate and lithium phosphate crystals of 2 to 4 μm average size.

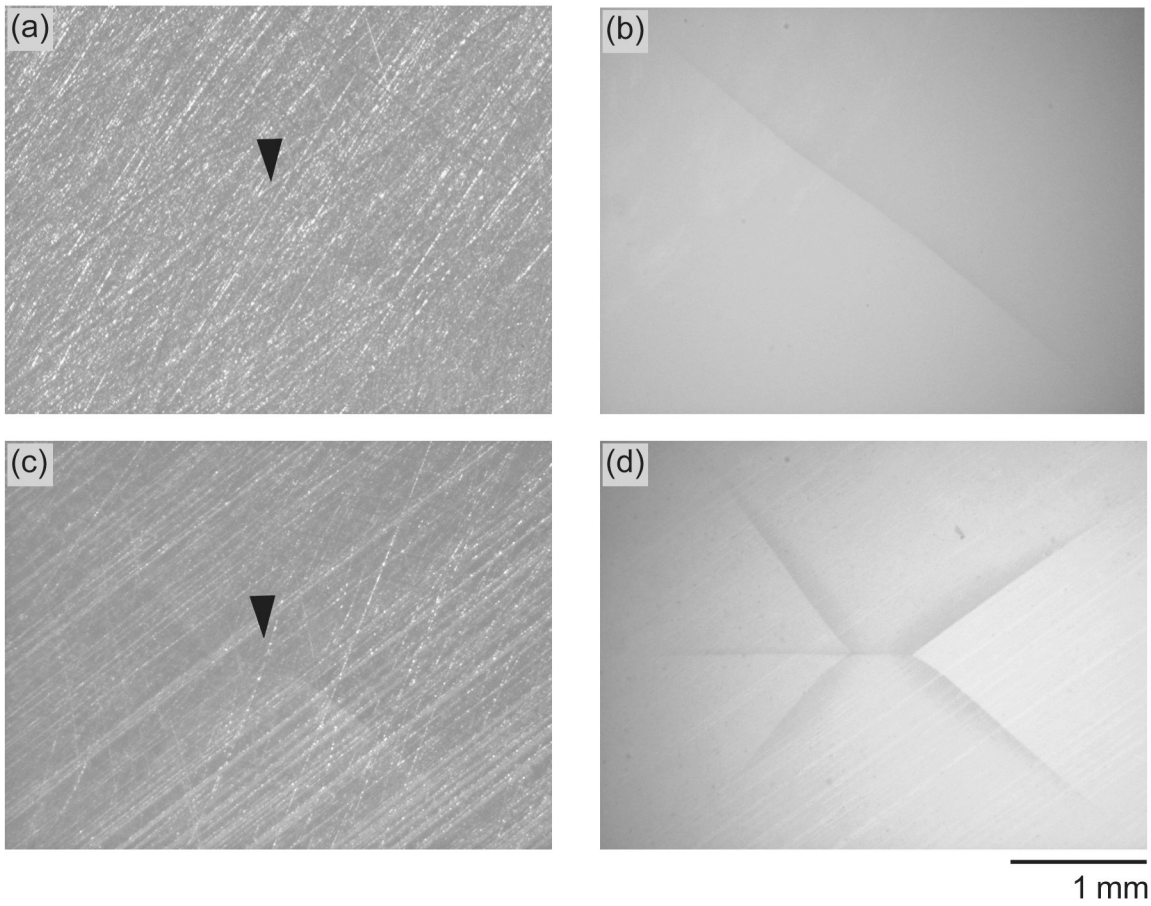

Figure 3.

Representative stereo optical microscopy images show surface features of (a) 3Y-TZP and (c) 5Y-PSZ discs fractured at 1010 N and 774 N, respectively. Images were obtained using reflected light illumination. Arrows indicate the contact area, demonstrating the absence of near-contact induced top surface cone cracks. (b) and (d) are images of the same specimens, but acquired using transmitted light illumination to reveal the far-field flexural induced radial cracks initiated at the cementation surface of the ceramic discs. Images were taken on ceramic discs that have been “peeled off” of their dentin analog composite substrate after the Hertzian load-to-fracture test.

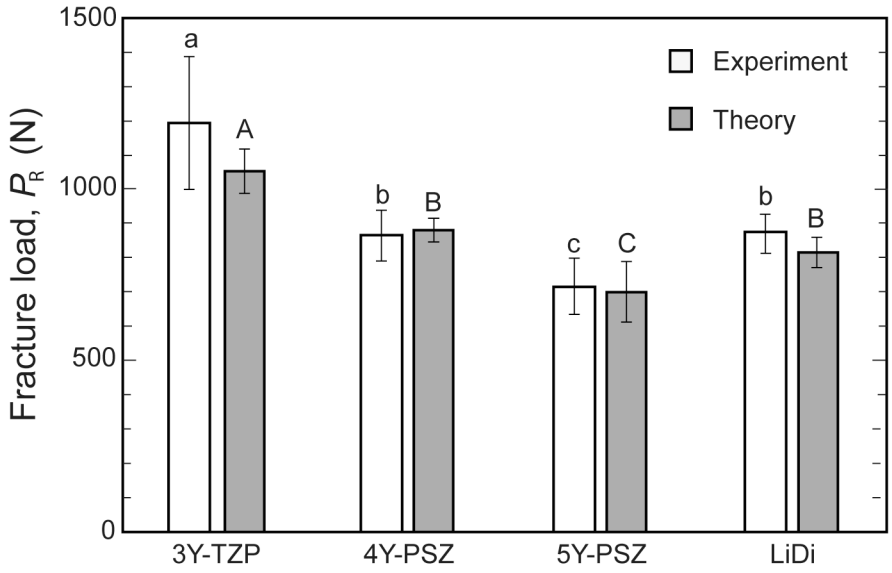

Figure 4.

Theoretical and experimental load-bearing capacity of zirconia and lithium disilicate for the trilayer systems—ceramic/cement/dentin-like substrate. Different upper and lower-case letters indicate a statistical difference among materials for theory and experiment, respectively.

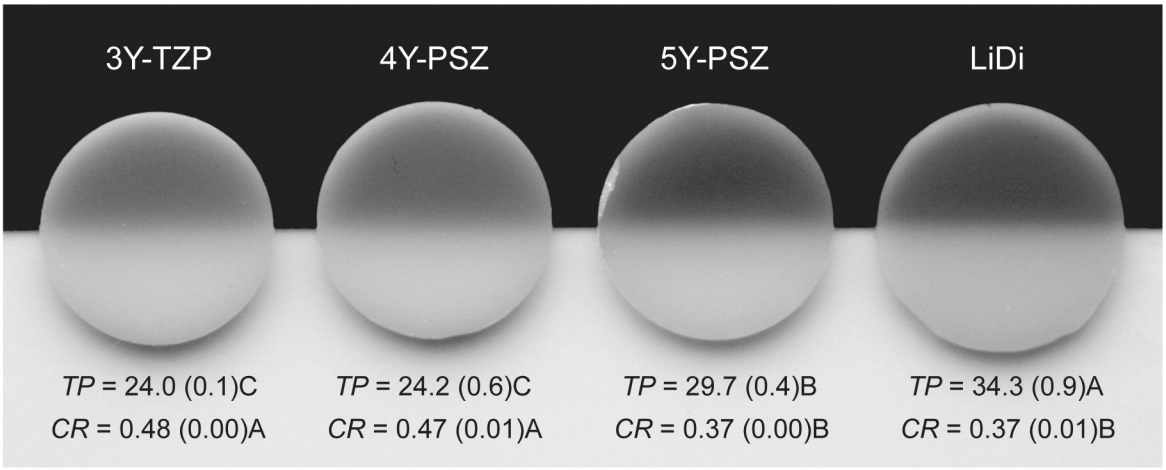

Figure 5.

Digital photograph illustrating the comparative translucency of the four materials at 1 mm thickness. Average (standard deviation) of translucency parameter (*TP*) and contrast ratio (*CR*). Different letters indicate statistical difference among materials, within each property.

Table I.

Properties of materials used in this study.

Material	Manufacturer	Sintering condition	Composition (%)	Modulus, $E^{\dagger}$ (GPa)	Strength, σ (MPa)	Thickness, d/h (mm)
Zirconia						
Zpex (3Y-TZP)	Heany Dental	1530°C for 2h	*t*-ZrO_2: 71, *c*-ZrO_2: 29	210	904 (57) A	1.0 ± 0.2
Zpex 4 (4Y-PSZ)	Heany Dental	1450°C for 2h	*t*-ZrO_2: 43, *c*-ZrO_2: 57	210	749 (29) B	1.0 ± 0.2
Zpex Smile (5Y-PSZ)	Heany Dental	1450°C for 2h	*t*-ZrO_2: 31, *c*-ZrO_2: 69	210	593 (90) C	1.0 ± 0.2
Glass-ceramic						
IPS e.max CAD	Ivoclar Vivadent	820°C for 2 min + 840°C for 7 min	Crystals: 70, Glass: 30	95	488 (28) C	1.0 ± 0.2
Cement						
Multilink Automix	Ivoclar Vivadent	Light cured	Glass, DMA, HEMA	7.9	114 †	0.04 ± 0.01
Composite						
G10	Acculam	Lab fabricated	Glass fiber, Epoxy	18.6	379 †	15

†Data from manufacturers.

Different letters indicate statistical difference among materials, within each property.